Speckle imaging with a partitioned aperture: experimental results

Brandoch Calef
Boeing LTS Maui, 535 Lipoa Parkway Suite 200, Kihei HI 96753

ABSTRACT

Speckle imaging techniques make it possible to do high-resolution imaging through the turbulent atmosphere by collecting and processing a large number of short-exposure frames. In severe conditions, when the diameter of the telescope is much larger than the characteristic scale of atmospheric fluctuations, the reconstructed image is dominated by "turbulence noise" caused by redundant baselines in the pupil. In earlier work, it was shown that this noise could be dramatically reduced by partitioning the telescope aperture and combining the bispectra of all the subapertures. We report the results of an experiment using the GEMINI sensor on the 1.6-meter telescope at the Maui Space Surveillance Site.

1. INTRODUCTION

An image collected through atmospheric turbulence is subjected to an unknown blur. The blur changes rapidly, so that in long-exposure images the higher spatial frequencies are wiped out. One way of dealing with this problem is to correct the wavefront in real-time using adaptive optics. A complementary approach is to use speckle imaging techniques, in which an image is reconstructed from many short exposures, each of which contains information out to the diffraction limit. This paper concerns the latter approach.

In previous work [1], we developed the idea of aperture partitioning, which involves splitting the pupil into several regions and making simultaneous focal-plane measurements from the light in each one. This is similar to aperture-masking interferometry, which masks out everything but a thin annulus at the outer edge of the pupil, except that no photons are sacrificed to the mask. The point of either approach is to reduce the number of pairs of atmospheric cells (baselines) with the same vector separation in each subaperture. Redundant baselines reduce the SNR of the bispectrum estimate from which the object's Fourier phase is recovered. Reducing the redundancy therefore improves the quality of the reconstructed image. This was demonstrated in our earlier paper using simulation results. In this paper, we show experimental results using data collected on the 1.6 m telescope at the Maui Space Surveillance Site on Haleakala.

To fix notation and provide some background, we review bispectrum reconstruction. Let $h(x)$ be an atmospheric point-spread function (PSF) and let $o(x)$ be the object to be recovered. The measured data $d(x) = h(x) * o(x)$ is the convolution of the two. Using upper case to denote Fourier transforms, the data can be written $D(u) = H(u)O(u)$, where $H(u)$ is the optical transfer function (OTF). From this, one may recover $|O(u)|$ from the ratio of the ensemble averages of $|D(u)|^2$ and $|H(u)|^2$. However, this provides only the object's Fourier amplitude.

The phase can be obtained from the bispectrum, which is defined as

$$B_D(u, v) = D(u)\, D(v)\, D^*(u + v). \tag{1}$$

It is easy to see that $B_D(u, v) = B_H(u, v)B_O(u, v)$. The key result in speckle imaging is that the ensemble average of the bispectrum of the atmospheric PSF has zero phase, so $\arg B_O(u, v) = \arg \mathbb{E}[B_D(u, v)]$.

The rate at which the phase of the atmospheric bispectrum converges to zero depends strongly on the ratio of the telescope diameter D to Fried's parameter r_0. The latter may be thought of as the characteristic size of atmospheric cells over which the phase is roughly constant. The number of cells in the pupil is therefore about $(D/r_0)^2$. As turbulence strength rises, r_0 drops and the density of cells in the pupil increases. This increases the degree of baseline redundancy, which reduces the efficiency of phase closure in Eqn. 1. Partitioning the aperture counters this effect, resulting in better phase estimates, especially when D/r_0 is large. To combine the information from the partitions, the bispectrum is estimated from each one and then averaged together, weighted by SNR.

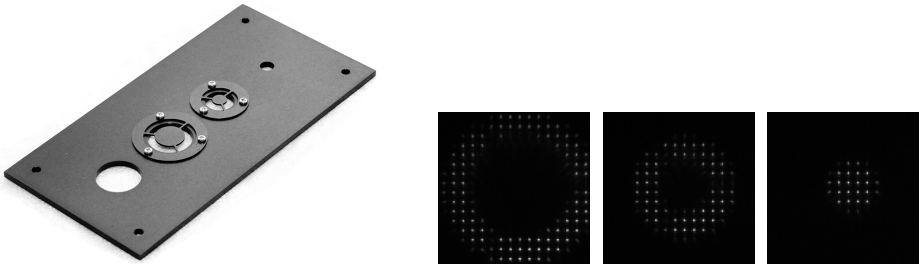

(a) (b)

Figure 1. Pupil masks. (a) Aperture mask plate installed in the sensor. (b) Shack-Hartmann images of each subaperture. Note that these were made with an internal source, so the secondary obscuration is not visible in the smallest mask.

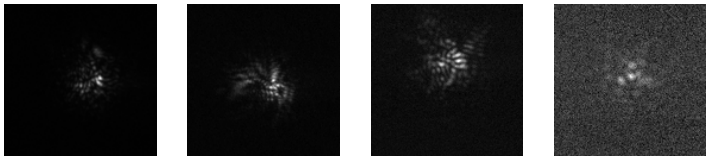

Full Outer Middle Inner

Figure 2. Data in each subaperture.

2. EXPERIMENTAL DESIGN

We tested this concept using the GEMINI sensor on the MSSS 1.6 m telescope, which is capable of collecting critically-sampled imagery at over 200 Hz. To be operationally useful, a phase mask or mirror arrangement would be needed to partition the aperture so that all subapertures could be measured simultaneously. However, as an initial demonstration, we instead used a series of pupil masks to measure each subaperture in succession. This is a valid demonstration, since the bispectrum of each subaperture is estimated independently. However, it cannot be applied to LEO satellites, since the object pose changes noticeably in the time required to switch masks.

A set of four pupil masks were made in a steel plate (see Fig. 1a) and mounted on a motorized linear stage at a pupil in the system. Switching from one mask to another can be done from the sensor console and takes about two or three seconds. The masks include the full pupil and three annular subapertures. The outermost mask spans the entire 1.57 m pupil, the middle annulus has an outer diameter of 1.05 m, and the inner annulus is 0.53 m across. Within the inner annulus is the central obscuration of the telescope, which is 0.36 m across. Thus, the inner annulus has a thickness of about 8.5 cm and the middle and outer annuli are about 26 cm thick. Wavefront sensor images of each subaperture are shown in Fig. 1b.

In order to get a wide range of conditions, data was collected over two days (once in mid-morning and once in mid-afternoon) and three nights (all evening terminator). Stars were collected at elevation angles between 20 and 85 degrees. A variety of filters were used, typically in the 700-900 nm range. For each data set, seeing was estimated from the short-exposure imagery using the technique of von der Lühe [2]. Median daytime seeing was 3 cm and median nighttime seeing was 8 cm.

Fig. 2 shows data collected in each mask.

3. RESULTS

To compare the relative performance of full-aperture and partitioned-aperture speckle imaging, quasi-experimental data is synthesized from the collected stars. This is accomplished by convolving each star frame (p) with a TASAT rendering of SEASAT (o), normalized to $\sum o_i = 1$. One can see that this does not have valid photon statistics, so Gaussian noise with variance $(o - o^2) * p$ was added to each image. This approximately corrects the statistics.

To form a reconstruction from the three-subaperture data, the bispectrum is estimated from the first N frames of each of the three masks. The object Fourier phase is recovered from the weighted average of the bispectra.

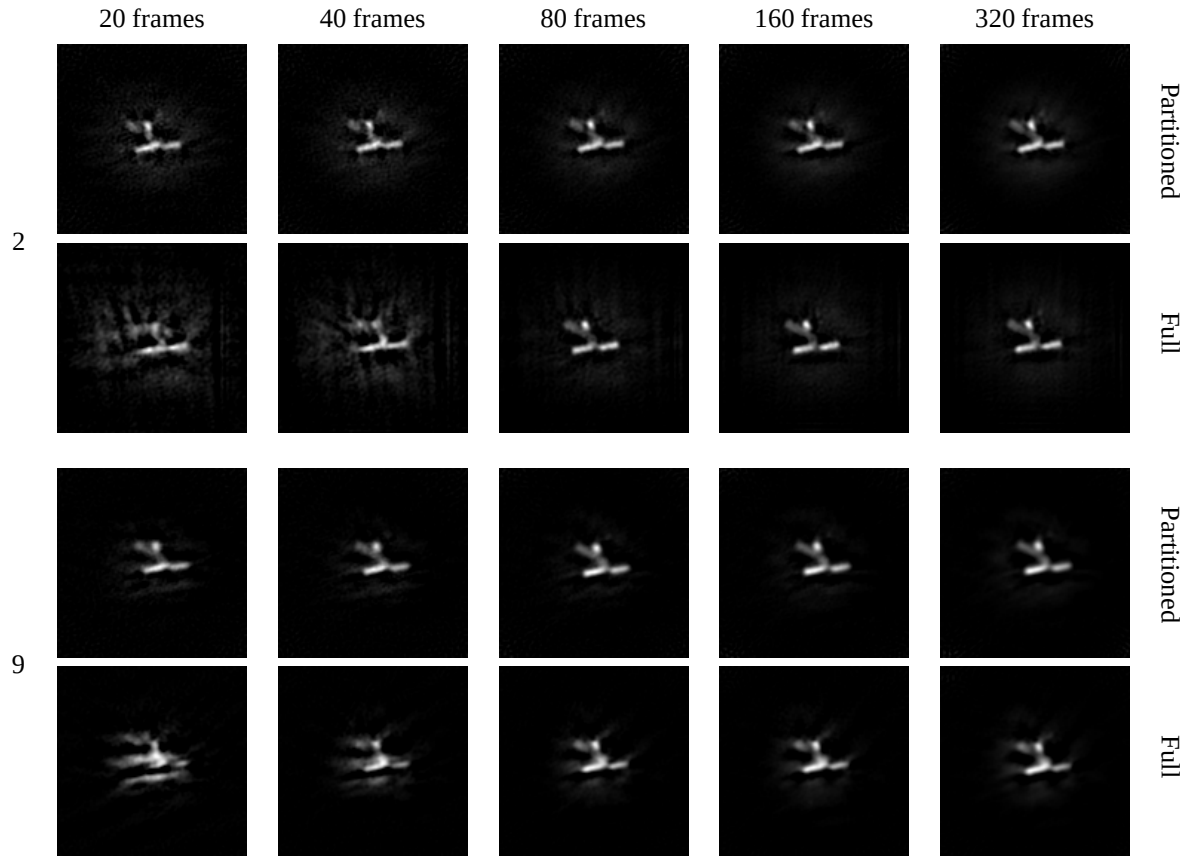

Figure 3. Reconstructions for data sets 2 and 9 (both collected during daytime; see Table 1 for more information).

To form a reconstruction from the full-pupil data, three groups of $N/3$ consecutive frames are used. The groups are spaced several seconds apart. The purpose of this is to ensure that the partitioned-aperture method does not derive some advantage from the fact that the atmosphere has time to decorrelate while the pupil mask in the sensor is being changed.

Some example reconstructions are shown in Figs. 3 and 4. For most data sets, aperture partitioning produces a visually preferable result. In order to better quantify this, a second set of extended data is created using a resolution target as the pristine object. Then each reconstruction is visually assessed to determine the minimum resolvable feature size in pixels. The results of this operation for each data set are shown in Table 1 and the plot in Fig. 5.

Two trends are apparent in these results. First, more severe seeing conditions (smaller r_0) consistently favors aperture partitioning. In particular, aperture partitioning produced a better result for all but one of the daylight data sets. This is consistent with the view that there is a tradeoff between redundancy noise and sensor noise. Using a partitioned aperture reduces redundancy noise, but by dividing the light among three separate focal planes, it experiences more sensor noise. As r_0 drops (as in the daytime, for example), redundancy noise becomes dominant. But in good seeing conditions, the lower sensor noise in the full-aperture data produces a better result.

Second, as more frames are processed together, the two methods tend to approach the same resolution. This is because the atmosphere is decorrelating, allowing the full-aperture case to beat down the redundancy noise. In practice, the number of frames that can be processed together is dictated by the rate at which the object (the satellite) is changing pose.

Both of these observations are consistent with the simulation results we reported last year. They suggest that the best application of aperture partitioning is for very severe seeing, especially with a rapidly evolving target.

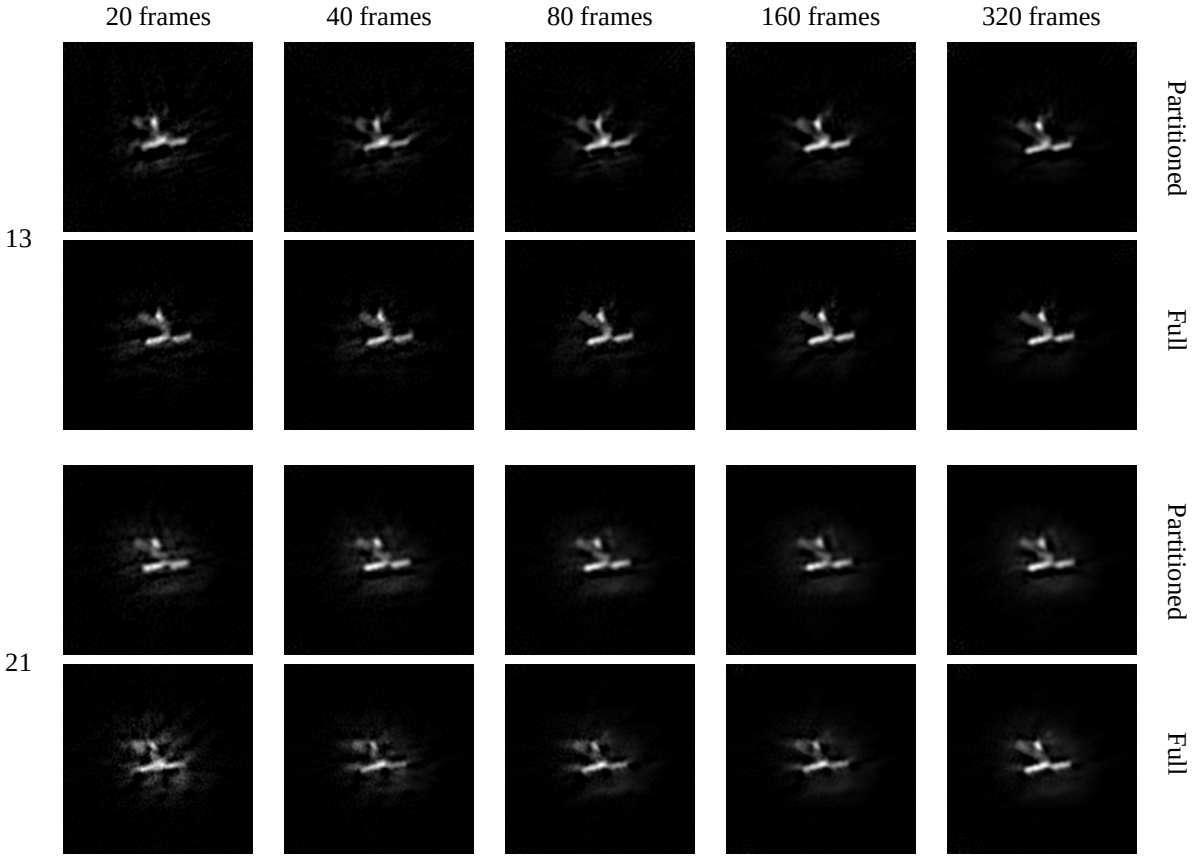

Figure 4. Reconstructions for data sets 13 and 21 (both collected during evening terminator; see Table 1 for more information).

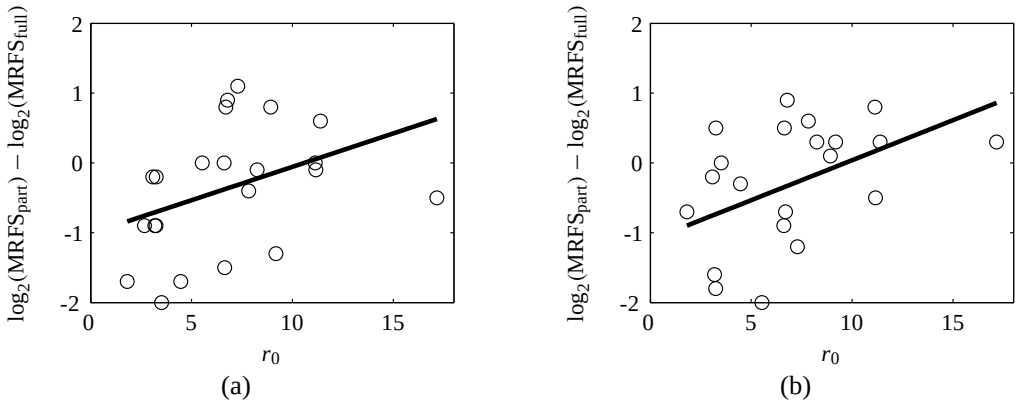

Figure 5. Difference in $\log_2$ of minimum resolvable feature size vs r_0 for (a) 20 frames and (b) 320 frames. Negative values indicate cases in which aperture partitioning produced the better result. Its advantage tends to diminish as r_0 increases.

Table 1. Summary of data sets, sorted by local hour. Data sets 1–11 were collected during daylight, 12–24 were after sunset. Shown are the minimum resolvable feature size (MRFS) in pixels for partitioned and full aperture, and as a function of the number of frames in the processing ensemble. Cases judged to be unresolved (MRFS$\geq$ 40) are marked *U*.

				MRFS (Partitioned)					MRFS (Full aperture)				
Dataset	r_0 (cm)	PSNR	Local time	20	40	80	160	320	20	40	80	160	320
1	3.2	20	09:40	14	5.5	3.1	2.3	2.3	27	15	12	25	7.0
2	1.8	14	09:42	12	10	6.0	3.7	3.4	*U*	*U*	5.5	5.5	5.5
3	4.7	6	09:54	*All unresolved*					*All unresolved*				
4	3.3	24	10:04	34	32	32	22	30	*U*	34	22	30	22
5	2.9	14	10:06	*U*	*U*	*U*	38	38	*U*	*U*	*U*	38	38
6	2.7	35	10:09	22	10	10	10	4.7	*U*	*U*	*U*	22	22
7	5.5	26	15:59	10	7.0	7.0	4.7	3.7	10	5.5	8.2	27	14
8	3.2	39	16:02	22	10	4.7	3.7	3.7	*U*	*U*	22	22	13.2
9	3.5	26	16:19	5.5	4.7	4.7	4.7	4.7	22	22	4.7	4.3	4.7
10	6.6	13	16:48	*U*	*U*	20	5.5	5.1	*U*	*U*	22	10	9.7
11	7.3	30	16:51	19	15	5.1	4.7	4.7	8.9	5.5	4.7	5.5	10
12	6.6	52	19:30	5.5	4.3	4.3	2.5	3.1	15	2.7	2.5	2.3	2.3
13	6.8	20	19:33	22	22	6.5	4.7	4.7	11	9.7	4.7	3.1	2.5
14	3.1	18	20:13	36	15	4.0	3.1	3.1	*U*	30	5.5	4.0	3.7
15	17.2	40	20:15	3.1	2.9	2.1	1.4	1.3	4.3	4.0	2.3	1.4	1.1
16	8.9	24	20:25	8.2	3.7	2.1	2.3	1.8	4.7	3.1	2.3	2.1	1.7
17	11.4	50	20:28	6.5	4.7	4.0	3.1	2.1	4.3	2.3	1.8	1.8	1.7
18	6.7	30	20:34	9.7	4.7	4.3	2.9	2.5	5.5	4.7	4.7	4.7	4.0
19	8.3	55	20:37	3.4	2.3	2.3	1.7	1.7	3.7	2.7	2.5	2.3	1.3
20	9.2	38	20:38	4.3	2.1	1.9	1.9	1.8	10	2.5	2.1	1.7	1.4
21	4.5	31	20:39	4.7	4.0	2.3	2.3	2.3	15	6.5	5.5	3.1	2.9
22	11.1	38	20:42	4.7	4.3	2.5	3.1	2.3	4.7	3.7	2.5	2.1	1.3
23	7.8	33	20:47	5.5	4.0	2.1	1.9	2.1	7.0	4.7	3.4	2.3	1.4
24	11.2	26	20:56	5.1	4.3	3.1	2.9	1.7	5.5	4.3	2.5	2.3	2.3

4. NEXT STEPS

We conclude by saying a few words about another aperture partitioning experiment that is in preparation, this one on the AEOS 3.6 m telescope. This one will incorporate a phase mask that puts different amounts of tilt on different parts of the pupil, causing the annular subapertures to form images on separate parts of the focal plane. In this way, all the subapertures can truly be measured simultaneously. Moreover, we will use a beamsplitter to make simultaneous full-aperture measurements using a second camera to allow comparison of the two techniques with satellite passes.

This experiment will have some other important advantages over the GEMINI experiment described here. It will use EMCCDs to collect speckle images, driving the effective read noise to well under 1 e^- per pixel. It will have a wider field of view, so the data will not be truncated so badly at the edge of the array when seeing conditions are bad. It will also have a much better tracker, which will also help.

ACKNOWLEDGMENTS

Invaluable engineering support was provided by Chris Young, Chris Shurilla, and Ed Walker. This work was funded by the Air Force Office of Scientific Research through AFRL contract FA9451-05-C-0257.

REFERENCES

[1] Calef, B. and Therkildsen, E., "Improving large-telescope speckle imaging via aperture partitioning," in [*Proceedings of the AMOS Technical Conference*], (2008).

[2] von der Lühe, O., “Estimating Fried’s parameter from a time series of an arbitrary resolved object imaged through atmospheric turbulence,” *Journal of the Optical Society of America A* **1**(5), 510–518 (1984).